

Unprecedented arsenic photo-oxidation behavior of few- and multi-layer $Ti_3C_2T_x$ nano-sheets

Maibelin Rosales ^{a,b}, Andreina Garcia ^{a,*}, Victor M. Fuenzalida ^c, Rodrigo Espinoza-González ^b, Guichen Song ^d, Bo Wang ^d, Jinhong Yu ^d, Francisco Gracia ^b, Andreas Rosenkranz ^{b,*}

^a Advanced Mining Technology Center (AMTC), Universidad de Chile, 8370451 Santiago, Chile

^b Department of Chemical Engineering, Biotechnology and Materials, FCFM, Universidad de Chile, Santiago, Chile

^c Department of Physics, FCFM, Universidad de Chile, Santiago, Chile

^d Key Laboratory of Marine New Materials and Related Technology, Zhejiang Key Laboratory of Marine Materials and Protection Technology, Ningbo Institute of Material Technology & Engineering, Chinese Academy of Sciences, Ningbo 315201, PR China

ARTICLE INFO

Article history:

Received 16 May 2020

Revised 3 July 2020

Accepted 17 July 2020

Keywords:

$Ti_3C_2T_x$ nano-sheets

Mxenes

Photo-oxidation

As removal

Water purification

ABSTRACT

Water contaminated by arsenic is a tremendous risk for health and environment due to its toxic and carcinogenic nature thus asking for more advanced and efficient removal strategies. Therefore, the aim of this study is to investigate for the first time the photo-oxidation performance of few- and multi-layer $Ti_3C_2T_x$ nano-sheets (Mxenes) regarding the arsenic removal from synthetic arsenic solutions. Few-layer Mxene nano-sheets have the capability to efficiently oxidize highly toxic As(III) to less harmful As(V) and possess at the same time a notable adsorption capability for both species (about 44% for As(III) and 50% for As(V)). The quantification of photogenerated hydroxyl radicals verified that few-layer Mxene nano-sheets are capable to generate 4 times more hydroxyl radicals compared to multi-layer Mxene nano-sheets. The increase amount of produced $\cdot OH$ radicals observed for few-layer Mxene nano-sheets can be attributed to its higher content of available active TiO_2 sites, which provide more redox reaction sites thus improving the photocatalytic behavior. Moreover, the detected -OH surface terminations verified on the few-layer MXene nano-sheets promote their significant adsorption capacity. Thereby, our results demonstrate that especially few-layer Mxene nano-sheets are a promising candidate for an efficient arsenic removal due to its unprecedented dual effect of adsorption/photo-oxidation regarding this toxic contaminant.

© 2020 Elsevier Ltd. All rights reserved.

1. Introduction

Water contaminated by arsenic (As) represents a significant environmental and public health problem in more than 50 countries around the globe including United States, India, China, Mexico, among others due to the toxic and carcinogenic nature of As. In aqueous systems, arsenic is commonly present as arsenite (As(III)) and arsenate (As(V)). Comparing both species, it can be stated that arsenite is more harmful and more difficult to be removed [1,2]. Notable research effort has been dedicated to explore technologies to efficiently remove arsenic from water. For instance, approaches based upon the oxidation of As(III) to As(V)

using chlorine, permanganate or oxygen followed by coagulation-electrocoagulation/precipitation processes employing aluminum or ferric salts, and sedimentation/filtration have been proposed [2,3]. Moreover, adsorption with novel materials such as alumina, activated carbon, iron oxides, activated biochar, among others, have been also investigated [1,2,4,5]. Additionally, physical/chemical processes including ion exchange, membrane technologies and biological treatments are also used [1,2]. These technologies can be even combined to fulfil rather strict water quality standards as established by the World Health Organization (WHO) ($<10 \mu\text{g}\cdot\text{L}^{-1}$) [1,2].

In this context, the oxidation of the more toxic As(III) to the less harmful As(V) may be a required step in processes for water treatment. Thus, advanced oxidation methods such as heterogeneous photocatalysis using a photoactive semiconductor have been proposed due to their low cost and possibility of using solar radiation as an energy source [6,7]. Until now, titanium dioxide (TiO_2) has been mostly used due to its excellent chemical stability, low cost,

* Corresponding authors.

E-mail addresses: maibelin.rosales@amt.c1 (M. Rosales), andreina.garcia@amt.c1 (A. Garcia), vfuenzal@ing.uchile.cl (V.M. Fuenzalida), roespino@ing.uchile.cl (R. Espinoza-González), songguichen@nimte.ac.cn (G. Song), wangb@nimte.ac.cn (B. Wang), yujinhong@nimte.ac.cn (J. Yu), fgracia@ing.uchile.cl (F. Gracia), arosenkranz@ing.uchile.cl (A. Rosenkranz).

nontoxicity, high oxidizing power, and, especially, its electronic as well as optical properties [7]. It is well known that many factors influence the photocatalytic performance of TiO_2 , such as band gap, particle size, specific surface area, porous structure, crystalline phase, and exposed surface facets. Moreover, it has been demonstrated that the photocatalytic activity also depends on the concentration of reactive oxygen species (ROS) that the photocatalyst is capable to generate [8,9].

In order to improve the photocatalytic activity of TiO_2 , different modifications of the photocatalyst including its doping with metals and non-metals [10,11], the formation of heterojunctions by combining it with other semiconductors [12], photosensitization [8], the modification of exposed facets [13], the formation of structural defects (in particular oxygen vacancies) [14], and the synthesis of nano-sized structures [7,15–17] have been investigated. Additionally, some studies have verified the influence of the photocatalyst's morphology and dimensionality on the photocatalytic performance [8,12,18].

Consequently, 2D TiO_2 photocatalysts have gained considerable attention in the last few years due to their excellent adsorption capacities, uniform morphology, high specific surface area, and low thickness thus improving the separation rate of generated electron-hole pairs [11,19,20]. Its smooth and regular surface topology enables a strong interaction between the reactants and the TiO_2 sheets thus enhancing ROS production and the photocatalytic efficiency [21]. It is worth mentioning that 2D TiO_2 have demonstrated superior photocatalytic activity than TiO_2 in other morphologies, since short diffusion pathways in the ultra-thin sheets suppress the recombination of photo-excited electron-hole pairs during photocatalysis [22]. Moreover, graphene- TiO_2 nanocomposites (GR- TiO_2) have been explored in the photocatalytic oxidation of benzylamine under visible light. The bi-dimensional morphology resulting from the combination of both 2D materials (graphene and TiO_2) exhibited a greater interfacial contact, which enhanced the separation and transfer of generated electron-hole pairs, thus boosting catalytic activity [23].

In the last couple of years, the family of 2D materials has been significantly extended by early transition metal carbides and/or carbonitrides (Mxene nano-sheets), which bear tremendous potential to serve as photocatalysts. Discovered by Gogotsi's group in 2011, the first synthesis of $\text{Ti}_3\text{C}_2\text{Tx}$ nano-sheets, which can be considered as the most explored Mxene family member, has been realized by selectively removing the "A" layers of Ti_3AlC_2 , which is the corresponding MAX-phase [24]. In this regard, the Mxene synthesis is typically based upon MAX-phases with the general chemical formula $\text{M}_{n+1}\text{AX}_n$, where M represents an early transition metal, A stands for a group IIIA or IVA element and X is either C or N. The sub-index n can take values of 1, 2 and 3 [24,25]. Since the initial synthesis using highly concentrated HF, numerous studies have been dedicated to find alternative and less harmful etching routes thus ending up in procedures making use of mixtures of HF with HCl as well as HCl and LiF or molten salts (LiF + NaF + KF) among others [26–30]. Nowadays, it is possible to exfoliate the synthesized Mxene nano-sheets thus enabling the fabricating of multi-, few-, bi- up to single-layer Mxene nano-sheets by the intercalation of larger molecules or ions or by ultrasonication [25,29,31]. Due to the involved processes, Mxene nano-sheets are typically terminated with different surface groups including -O, -OH and -F terminations [32]. Since the discovery, Mxene nano-sheets in general and particularly $\text{Ti}_3\text{C}_2\text{Tx}$ nano-sheets have gained tremendous attention due to their outstanding material's performance in energy storage [33–36], catalysis [37–39], tribology [40–43], water treatment [44,45] and advanced composites [46–48].

Considering the photocatalytic activity, the research community has recently started to explore these properties on mainly multi-layer $\text{Ti}_3\text{C}_2\text{Tx}$ nano-sheets. In this regard, it must be pointed out

that the majority of presented studies made use of hybrid Mxene systems, which include Mxene nano-sheets doped by Fe_2O_3 , BiOBr , Gd and Sn [49,50], and composites or co-catalyst systems such as $\text{TiO}_2/\text{Ti}_3\text{C}_2\text{Tx}$, doped- $\text{TiO}_2/\text{Ti}_3\text{C}_2\text{Tx}$ $\text{TiO}_2@\text{Ti}_3\text{C}_2/\text{g-C}_3\text{N}_4$, $\text{BiOBr}/\text{Ti}_3\text{C}_2$, $\text{g-C}_3\text{N}_4/\text{Ti}_3\text{C}_2$, $\text{CdS}/\text{Ti}_3\text{C}_2\text{Tx}$, and $\text{Co}_3\text{O}_4/\text{MXene}$ [51–57]. Moreover, $\text{Ti}_3\text{C}_2\text{Tx}$ nano-sheets have been utilized to explore the photodegradation of organic molecules, such as dyes [49–51,56–58], phenol [52,57], aromatic nitro compound [53], and pharmaceutical compounds [54,55]. Additionally, multi-layer Mxene nano-sheets have been also tested in the photoreduction of chromium [57,59]. However, photocatalytic reactions using pure few- and multi-layer Mxene nano-sheets as photocatalysts have been scarcely reported in literature. In addition, to the best of our knowledge, there is no experimental study on the performance of Mxene nano-sheets regarding their ability to remove As from water neither by adsorption nor photo-oxidation processes.

Therefore, the aim of this study is to assess the photo-oxidation performance of few- and multi-layer Mxene nano-sheets regarding their As removal capabilities from contaminated water. For this purpose, few- and multi-layer Mxene nano-sheets have been carefully characterized regarding their structural properties and surface chemistry using high-resolution techniques. Subsequently, few- and multi-layer Mxene nano-sheets have been added to arsenite solutions to study their As adsorption abilities without illumination and to evaluate their photo-oxidative performance from aqueous As(III) to As(V) under UVA illumination.

2. Materials and methods

2.1. Synthesis of few- and multi-layer Mxene nano-sheets

The initial Ti_3AlC_2 -powder was purchased from FORSMAN SCIENTIFIC Co. Ltd., Beijing (China). To synthesize multi-layer $\text{Ti}_3\text{C}_2\text{Tx}$ nano-sheets, 10 g of the Ti_3AlC_2 -powder were immersed in 100 ml of a 40% hydrofluoric acid solution. After mixing the solution in a magnetic stirrer at room temperature for 24 h, the suspension was washed with deionized water until a final pH of about 6 was reached. Afterwards, the suspension was centrifuged to separate the powder. Finally, the washed powder was filtered under vacuum conditions and dried at room temperature for 24 h. In case of the few-layer Mxene nano-sheets, 2 g of the as-synthesized dried multi-layer Mxene nano-sheets were added to distilled water and exfoliated by ultrasonication for one hour in an ice bath. Subsequently, the mixture was centrifuged at 2500 rpm for 10 min and, finally, filtered as well as dried under the aforementioned conditions.

2.2. Characterization of the few- and multi-layer Mxene nano-sheets

The structure, number of layers and the overall quality of the as-synthesized few- and multi-layer MXene nano-sheets were assessed using high-resolution transmission electron microscopy (HR-TEM, Tecnai F20, FEI). The acceleration voltage was kept constant at 200 kV. Energy dispersive X-ray spectroscopy using EDAX detector attached to the HR-TEM (TEM-EDX) was utilized to determine the chemical composition of the both nano-sheets. The overall surface chemistry was characterized by X-Ray diffraction (XRD) and Raman spectroscopy. In case of XRD, the respective diffractograms of the few- and multi-layer MXene nano-sheets were recorded using a powder diffractometer (PANalytical Empyrean) operating in Bragg-Brentano configuration at 40 kV and 40 mA with $\text{CuK}\alpha$ irradiation. An angular step size of 0.026° and the dwell time of 1396.89 s for each measuring point have been chosen. Considering Raman spectroscopy (Alpha 300 RA, Witec), few- and multi-layer MXene nano-sheets have been characterized using an excitation wavelength of 633 nm, a grating of 300 g/mm and 10%

of the maximum laser intensity. For both samples, 256 accumulations with an integration time of 4 s each have been used. X-Ray photoelectron spectroscopy (XPS, Physical Electronics 1257) using non-monochromatic AlK α and MgK α radiation has been utilized to characterize the surface chemistry of the few- and multi-layer MXene nano-sheets. Irrespective of the nano-sheets measured, the source was operating at 15 kV and 400 W with a pass energy of 44.75 eV for all scans. The surface composition was studied using an XPS wide scan with binding energies (BE) from 1000 to 0 eV using a step size of 1 eV, while narrow scans of the C_{1s}, F_{1s}, O_{1s} and Ti_{2p} regions were acquired using a step size of 0.1 eV. In case of the Ti_{2p} peak, a linear background subtraction was performed, while for all other peaks, the Shirley method has been utilized. The peaks were fitted using Lorentz-Gaussian functions.

2.3. Evaluation of the adsorption ability and photocatalytic activity of the few- and multi-layer Mxene nano-sheets

The photocatalytic activity of the few- and multi-layer MXene nano-sheets has been evaluated by photo-oxidative reactions of aqueous As(III) to As(V). Prior to reaction, 50 mg of the respective photocatalyst without any further pre-treatment were dispersed into 200 mL of a 1000 μ g/L arsenite solution. The As(III) stock solution was prepared by dissolving sodium-arsenite analytical grade (NaAsO₂) in distilled water, whose pH was adjusted to 7.0 with 0.1 mol/L hydrochloric acid or sodium hydroxide. The suspension was magnetically stirred without any illumination for 180 min to study the absorption behavior and to reach equilibrium conditions prior to irradiation (photo-oxidation). The experiments were conducted in a slurry batch reactor using a LuzChem LZC-4 V photo-reactor equipped with 14 lamps emitting in the UVA range. A constant distance of 10 cm was maintained between the lamps and the batch reactor, and the time of exposure was varied at 25 °C under continuous shaking. At specific times, 10 mL aliquots were taken and centrifuged. Then the supernatant was filtered through a Millipore membrane filter (pore size 0.22 μ m) to remove the photocatalytic material. Changes in the concentration of oxidized As(III) and photo-generated As(V) were determined using a colorimetric method [60,61]. The absorbance of the solution was measured at 890 nm utilizing an UV-Vis spectrophotometer [60,61]. The concentration of As(III) and photogenerated As(V) were obtained using calibration curves.

2.4. Determination of reactive oxygen species (ROS) – quantification of hydroxyl radicals (\bullet OH)

The formation of hydroxyl radicals (\bullet OH) by few- and multi-layer MXene nano-sheets under UVA irradiation was investigated and their concentration quantified by fluorescence spectroscopy employing the hydroxylation reaction of terephthalic acid (TA) in heterogeneous phase. TA is non-fluorescent, whereas the hydroxylated product 2-hydroxyterephthalic acid (2-HTA) is stable and highly fluorescent at 425 nm [62]. The corresponding reaction between the TA and the generated hydroxyl radicals to form 2-HTA is described in Eq. (1):



A TA solution (5×10^{-4} mol/L) was prepared by dissolving terephthalic acid in NaOH solution (2×10^{-3} mol/L). Prior to illumination, 0.05 g of the photocatalyst were dispersed into 50 mL of TA solution. Subsequently, the solution was magnetically stirred for 24 h without any illumination and then irradiated for 180 min under UVA light. For different irradiation times, an aliquot was taken and centrifuged at 15,000 RPM to separate the photocatalyst. Afterwards, the supernatant was removed and transferred to a quartz cuvette (1 cm optical path) for fluorescence analysis. Fluorescence

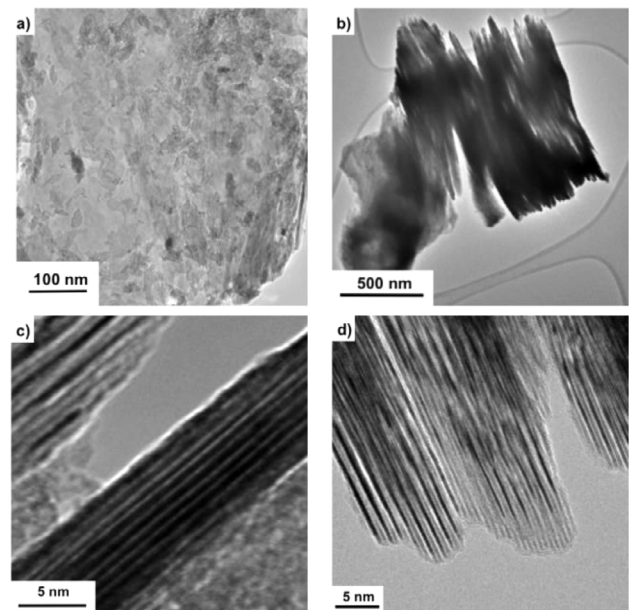


Fig. 1. (a and b) TEM-micrographs of individual few- and multi-layer nano-sheets with (c and d) their corresponding HR-TEM micrographs demonstrating their 2D layered structure. (a and c) represent the few-layer Mxene nano-sheets, while (b and d) display the multi-layer MXene nano-sheets.

spectra of 2-HTA were obtained using a Perkin Elmer LS55 fluorescence spectrophotometer at an emission wavelength of 425 nm using an excitation wavelength of 308 nm. The quantification of produced hydroxyl radicals was performed by relating the obtained fluorescence signals with the 2-HTA concentration using a calibration curve [8,9].

3. Results and discussion

3.1. Characterization of few- and multi-layer Mxene nano-sheets

HR-TEM has been used to assess the overall quality and structure of the as-synthesized few- and multi-layer MXene nano-sheets. The respective micrographs are exemplarily displayed in Fig. 1.

In Fig. 1a and b, pronounced contrast differences between the few- and multi-layer Mxene nano-sheets can be seen, which directly point towards a significantly different number of involved layers. This is further supported by the corresponding high-resolution micrographs displayed in Fig. 1c and d. The homogeneous and regular 2D structure can be clearly observed for both MXene nano-sheets, which have an averaged number of layers of about 10 (few-layers, left) and 70 (multi-layers, right), respectively. Cross-sectional analyses performed for both MXene nano-sheets revealed a layer-by-layer distance of about 0.91 ± 0.05 and 0.87 ± 0.07 nm for the few- and multi-layer Mxene nano-sheets, respectively. These values are in good agreement with previously published research work [63,64]. In order to quantify their chemical composition, TEM-EDX was performed on individual few- and multi-layer MXene nano-sheets. Irrespective of the number of layers, the detected main elements were titanium, carbon, oxygen and fluorine, whereas a minor contribution of aluminum was detected. However, the aluminum signal only accounted for about 0.3 wt.-%, which was therefore considered to be negligible. The observed elements in TEM-EDX fit well with the reported surface terminations when using selective HF etching to fabricate MXene nano-sheets [25,65].

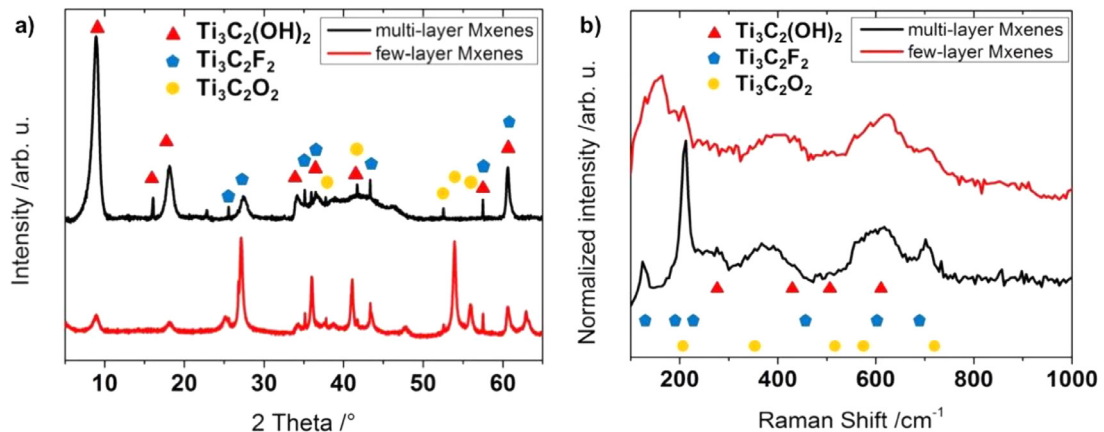


Fig. 2. Summary of the characterization results obtained by (a) XRD and (b) Raman spectroscopy for few- and multi-layer MXene nano-sheets.

To characterize the overall chemistry of the as-synthesized few- and multi-layer MXene nano-sheets, XRD and Raman spectroscopy have been performed. The respective results are summarized in Fig. 2.

The XRD spectra in Fig. 2a prove the existence of terminal groups (surface and interface), namely -OH, -O and -F contributions, for few- and multi-layer MXene nano-sheets. In this regard, it needs to be emphasized that only the relative amount of these functional groups varies depending on the number of layers. In case of the multi-layer MXene nano-sheets, the strongest signal stems from hydroxyl (-OH) groups, followed by weaker signals originating from -F and -O terminations. For the few-layer MXene nano-sheets, less pronounced contributions for -OH terminations can be observed, while stronger signals originating from oxygen and fluorine terminations can be detected. Following the simulated spectra of Hu et al. [66], the peaks assigned to different terminations consist of a mixture of simple hexagonal and Bernal stacking. When comparing the XRD spectra of both samples, a slight peak shift in the first diffraction peak can be seen, which points also towards a slightly increased layer-by-layer distance for few-layer MXene nano-sheets thus confirming the results obtained by HR-TEM.

The Raman spectra for few- and multi-layer MXene nano-sheets displayed in Fig. 2b support the XRD results. The Raman spectrum of the multi-layer MXene nano-sheets reveals pronounced, partially rather broad peaks at around 125, 212, 285, 376, 600 and 701 cm^{-1} . In accordance with the published research literature [32, 65–67], the detected Raman bands can be correlated with vibrations of $\text{Ti}_3\text{C}_2\text{O}_2$, $\text{Ti}_3\text{C}_2\text{F}_2$ and $\text{Ti}_3\text{C}_2(\text{OH})_2$, which goes hand in hand with the XRD and TEM-EDX results. Regarding the few-layer MXene nano-sheets, broad Raman peaks with contributions located at about 129, 159, 208, 381, 592, and 705 cm^{-1} , which can be again assigned to the aforementioned terminations. The synthesis-induced formation of $\text{Ti}_3\text{C}_2\text{O}_2$, $\text{Ti}_3\text{C}_2\text{F}_2$ and $\text{Ti}_3\text{C}_2(\text{OH})_2$ tends to change the respective lattice spacing, which results in additional, slightly shifted and possibly broadened Raman bands compared to the theoretical bands of solely Ti_3C_2 [32, 65, 66].

In order to characterize the surface chemistry of the few- and multi-layer Mxene nano-sheets, a detailed XPS analysis has been performed. The measured data with the corresponding peak fits and simulated spectra for the C_{1s} , O_{1s} , F_{1s} and Ti_{2p} peaks are summarized for both nano-sheets in Fig. 3.

Irrespective of the number of layers, the peak fitting for the C_{1s} component (Fig. 3 and b) required four different contributions with their most prominent one located at around 284.8 eV, which is typical for carbon in C-C chemical environment and adventitious carbon [68]. The peak located at 281.7 (281.8) eV for few-

layer Mxenes (multi-layer Mxenes) can be directly associated to C-Ti-Tx [68, 69], while the contribution at 286.5 eV can be traced back to organic components, particularly hydrocarbons [69, 70]. A minor contribution located around 288.5 eV can be detected for both few- and multi-layer Mxene nano-sheets, which is characteristic for C-F states [68]. When considering Fig. 3a and b as well as the respective values presented in Table 1, it can be stated that the energy positions of the different contributions match well for both samples investigated when taking the experimental error into consideration. This implies that the near-surface carbon bonding characteristics are fairly similar in few- and multi-layer Mxene nano-sheets.

The analysis of the O_{1s} peak (Fig. 3c and d as well as Table 1) demonstrates that this peak can be fitted by two contributions reflecting metal oxides and hydroxides. The latter can be directly connected to -OH surface terminations ($\text{C}-\text{Ti}-(\text{OH})_x$) [68, 69, 75]. When looking at the respective figures, it becomes evident that the relative amounts significantly change for few- or multi-layer Mxene nano-sheets. In this regard, few-layer Mxene nano-sheets contain about 55% of metal oxides (TiO_2 or more generally Ti(IV)), while the remaining 45% can be associated to hydroxides. In contrast, the contribution of hydroxides and metal oxides in multi-layer Mxene nano-sheets can be estimated to be about 90 and 10%, respectively. When having a detailed look at the values presented in Table 1, it can be seen that the binding energies assigned to metal oxides are fairly different (529.6 and 530.5 eV) for both samples. However, it is worth to mention that both energies can be associated to metal oxides according to [68]. In this sense, it is well known that oxidizing an element induces a positive charge thus requiring more energy to extract an electron and increasing the respective binding energy (displacement to the left in the spectrum). The reduction of an element, as oxygen, induces a negative charge, thus requiring less energy to extract an electron and decreasing its binding energy (displacement to the right in the spectrum). Regarding the metal oxide contribution, the higher binding energy observed for the few-layer Mxene nano-sheets suggests a "less reduced" O_{1s} , which can be associated to fluorine attached to titanium as oxyfluorides, since fluorine is more electronegative than oxygen and will capture the titanium electrons preferentially. Tanuma et al. reported on a slightly increased binding energy (0.2 eV) in the O_{1s} signal when studying titanium oxyfluoride as compared to titanium oxide [71]. Regarding the -OH contribution, it can be seen that only the relative amounts changed, while keeping the main binding energy constant.

The F_{1s} spectra for the few- and multi-layer Mxene nano-sheets (Fig. 3e and f) reflect two main contributions with rather similar binding energies, which can be correlated to fluorinated TiO_2

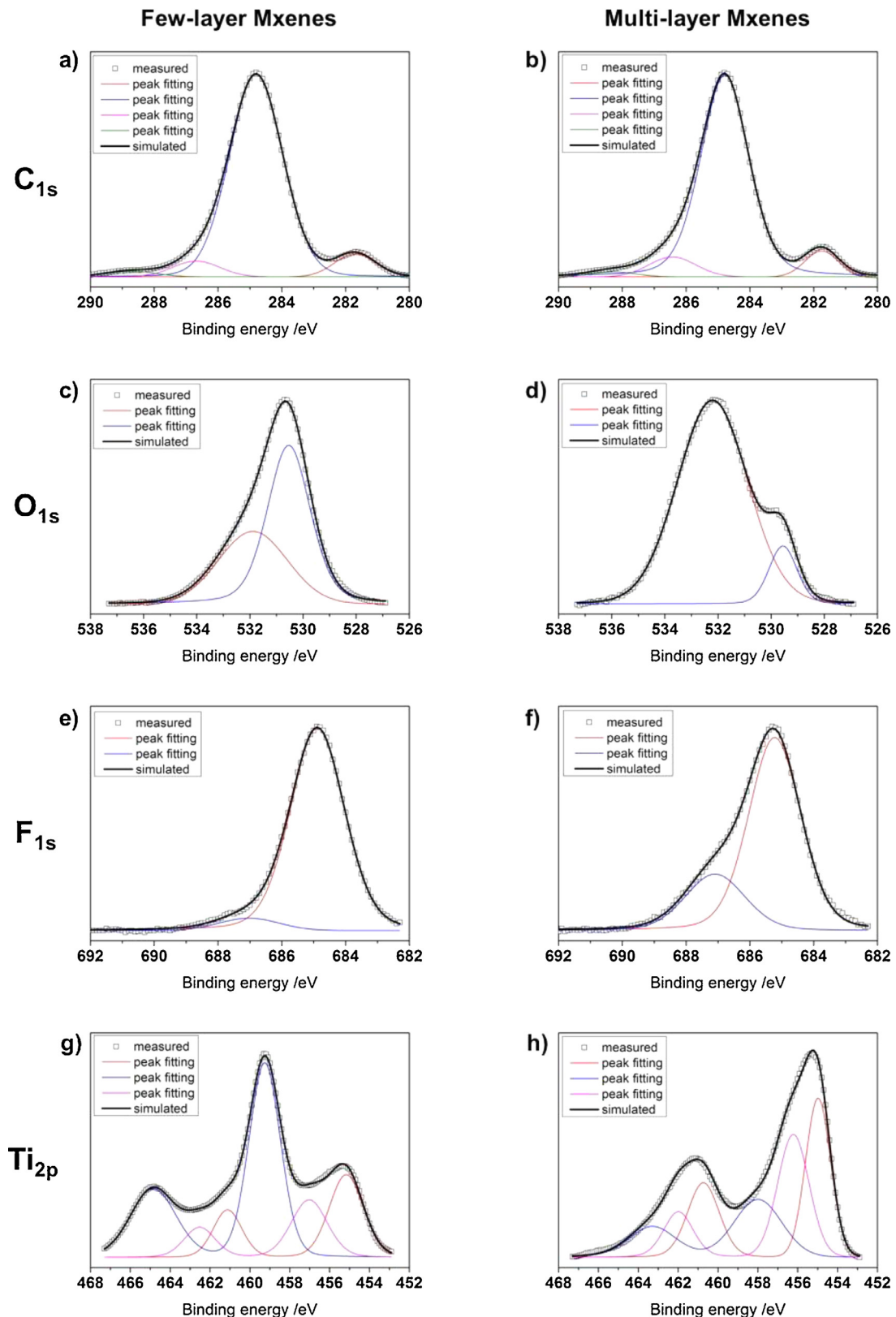


Fig. 3. Summary of the narrow XPS scans of the (a and b) carbon C_{1s}, (c and d) oxygen O_{1s}, (e and f) fluorine F_{1s} and (g and h) titanium Ti_{2p} peak recorded for (a, c, e and g) few-layer and (b, d, f and h) multi-layer Mxene nano-sheets (b, d, f and h). In all figures, the open squares represent the measured data, while the solid black lines resemble the simulated spectra after peak fitting. All individual contributions necessary to fit the experimental data are displayed in different colors.

Table 1

Summary of the peak fitting of all photoelectron peaks with their binding energies, FWHMs, fractions and assignments. The column "Elemental fraction" is the nominal contribution of each element to the spectrum.

	BE /eV	FWHM /eV	Peak fraction /%	Element fraction /%	Assignment	Reference
C_{1s}						
Few-layer Mxenes	281.7	1.5	7	52	C-Ti-T _x	[68,69]
	284.8	2.0	81		C-C, adventitious	[68]
	286.5	1.7	6		Hydrocarbons	[69,70]
	288.5	1.8	2		C-F states	[68]
Multi-layer Mxenes	281.8	1.2	7	70	C-Ti-T _x	[68,69]
	284.8	1.8	83		C-C, adventitious	[68]
	286.5	1.7	8		Hydrocarbons	[69,70]
	288.4	1.9	2		C-F states	[68]
O_{1s}						
Few-layer Mxenes	530.5	1.9	55 ± 6	29	Metal oxides Ti(IV)	[68]
	532.1	3.0	45 ± 6		C-Ti-(OH) _x	[68]
Multi-layer Mxenes	529.6	1.1	10	13	Metal oxides Ti(IV)	[68]
	532.2	3.0	90		C-Ti-(OH) _x	[68]
F_{1s}						
Few-layer Mxenes	684.9	2.0	94	7	TiO _{2-x} F _x	[71]
	686.8	2.2	6		C ₆ F ₆	[72]
Multi-layer Mxenes	685.2	1.9	75	9	TiO _{2-x} F _x	[71]
	687.1	2.2	25		C ₆ F ₆	[72]
Ti_{2p}						
Few-layer Mxenes	455.0	2.0	22	12	Titanium carbide (MXene)	[66,69,70,73]
	456.8	2.1	14		Ti(III)	[74]
	459.2	1.9	64		Ti(IV)	[74]
Multi-layer Mxenes	454.9	1.5	62	8	Titanium carbide (MXene)	[66,69,70,72]
	456.1	1.8	17		C-Ti-(O or OH)	[66]
	457.8	1.8	21		C-Ti-O	[66,69]

(TiO_{2-x}F_x) and fluorine in C₆F₆ [69,71]. For the few-layer Mxene nano-sheets, an increased signal for the species located at lower binding energies can be observed, thus suggesting stronger contributions of oxifluorides and less direct C-F bonds.

Fig. 3g and h demonstrate that three doublets have been used to fit the Ti_{2p} peak. For the multi-layer Mxene nano-sheets, the strongest contribution (62%) located at 454.9 eV can be assigned to titanium carbides (MXenes) [66,69,70,73], while two minor contributions centered at 451 and 457.8 eV can be connected to C-Ti-(O or OH) and C-Ti-O, respectively [66,69,70,73]. This assignment is in good agreement with the respective characterization results of XRD and Raman spectroscopy. However, for the few-layer Mxene nano-sheets, significant differences in the respective contributions and species have been detected. The carbide/Mxene contribution located at 455.0 eV largely decreased its contribution to only 22%. Moreover, contributions located at 456.8 and 459.2 eV have been detected, which can be traced back to higher oxidation states such as Ti(III) and Ti(IV) [74], respectively, which fits well with the observations made for the O_{1s} peak and the changed relative amounts.

3.2. Photocatalytic arsenic removal and ROS production of Mxene nano-sheets

The photocatalytic performance of few- and multi-layer Mxene nano-sheets has been investigated by an oxidation reaction of aqueous As(III) to As(V). The kinetics of the As(III) oxidation and its simultaneous transformation to As(V) for both materials are shown in Fig. 4a and b.

To study the adsorption capabilities of both nano-sheets, the first stage of the experiments was performed without any illumination. On the multi-layer Mxene nano-sheets, about 20% of the initial As(III) concentration have been adsorbed, whereas the few-layer Mxene nano-sheets adsorbed approximately 44% of the initial arsenite. The adsorption behavior of As(III) onto TiO₂-based materials has been explained by electrostatic attractive forces between arsenic (III) species and the material surface and/or physisorption processes due to its high surface area [76,77].

However, as can be seen by the presented characterization results, the surface terminations of both Mxene nano-sheets consists of -O, -OH, and -F groups, which implies a negatively charged surface [44]. Considering that the As(III) specie is present in the medium as a neutral molecule (H₃AsO₃⁰) at a working pH of 7, this implies a reduced affinity of the Mxene surface to the neutral H₃AsO₃⁰ specie. Moreover, no physisorption processes are expected to be less significant due to the low specific surface area measured for both materials (16.71 and 28.84 m²/g for few- and multi-layer Mxene nano-sheets, respectively). Consequently, it can be deduced that surface area and electrostatic forces are not the main driving factors controlling the adsorption capacity of As(III) by few- layer Mxene nano-sheets. A possible explanation for the observed adsorption behavior can be found in the formation of a monodentate complex between the neutral specie of As(III) and the -OH surface terminations present on the MXene nano-sheets. This goes hand in hand with results published for other materials having similar surface terminations [78,79].

After the analysis of the reactant's adsorption under dark conditions, the second stage was carried out under UVA illumination to study the photo-oxidative response of both nano-sheets. Under these conditions, the residual concentration of As(III) decreased, whereas the As(V) concentration continuously increased due to the involved oxidation processes. The complete photo-oxidation of As(III) to As(V) has been achieved after about 45 and 90 min of irradiation for few- and multi-layer Mxene nano-sheets, respectively.

The kinetic curves of the As(III) photo-oxidation have been fitted using pseudo-first-order kinetics (Fig. 5). In this context, the photo-oxidation rate of As(III) can be calculated as follows:

$$\ln(C_0/C_t) = k_{app} \cdot t \quad (2)$$

where C₀ is the initial concentration of the arsenite solution, C_t stands for the instant concentration of arsenite solution at the irradiation time t, and k_{app} (min⁻¹) represents the apparent photo-oxidation rate constant.

The k_{app} value of both Mxene nano-sheets after an irradiation time of 45 min as well as the linear regression coefficients are given in Table 2.

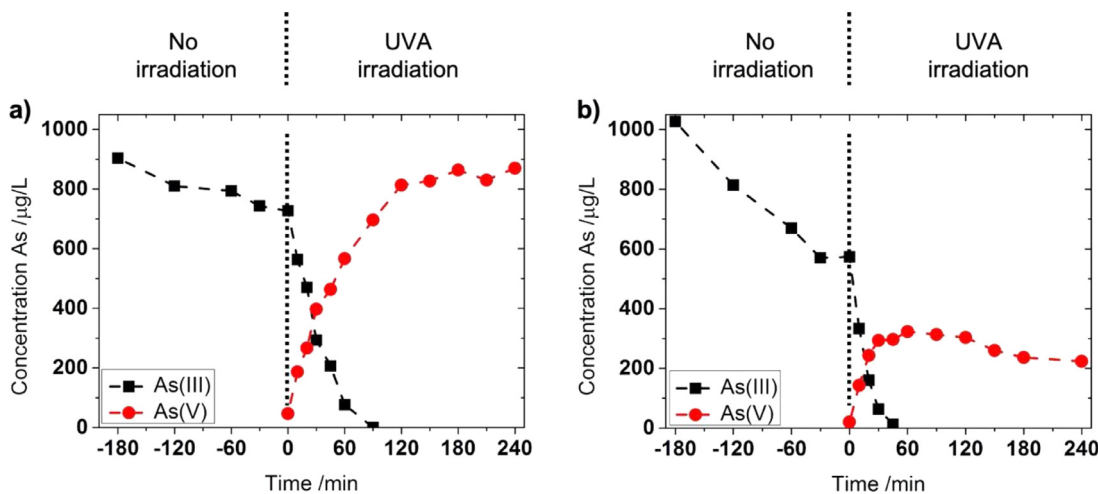


Fig. 4. Photo-catalytic performance of (a) multi-layer and (b) few-layer Mxene nano-sheets considering the oxidation of As(III) and the generation of As(V) using UVA irradiation at pH 7.

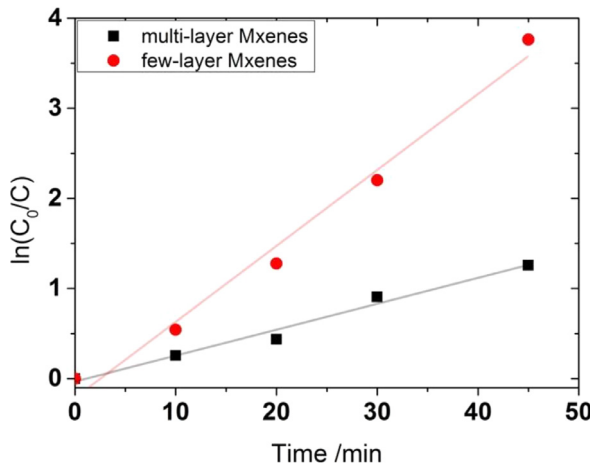


Fig. 5. The pseudo-first order kinetic model for the As(III) photo-oxidation for multi- and few-layer Mxene nano-sheets.

Table 2

Apparent pseudo-first-order reaction rate constant and linear regression coefficients (R^2) for the As(III) photo-oxidation induced by few- and multi-layer Mxene nano-sheets.

Sample	$k_{app} \times 10^{-2}$ (min ⁻¹)	R^2
Multi-layer	2.88	0.9821
Few-layer	8.43	0.9844

The linear relationship obtained between $\ln(C_0/C_t)$ and time as well as the k_{app} values summarized in Table 2 confirm that the few-layer MXene nano-sheets oxidize As(III) more quickly. The enhanced photocatalytic behavior observed for the few-layer MXene nano-sheets can be attributed to the increased amount of available active TiO_2 sites on its surface as verified by XPS. This observation agrees well with results published by Wang et al. [51]. Thus, under UVA irradiation, active TiO_2 sites present on the few-layer Mxene nano-sheets are excited to photo-generate electron/hole (e^-/h^+) pairs. The photo-generated electrons are rapidly transferred from the conduction band of TiO_2 to the Ti_3C_2Tx nano-sheets surface, which remarkably accelerates the separation of photogenerated carriers [80]. The high electrical conductivity of these nano-sheets due to their surface terminations can effectively improve the electron transport thus decreasing the recombination rate of e^-/h^+

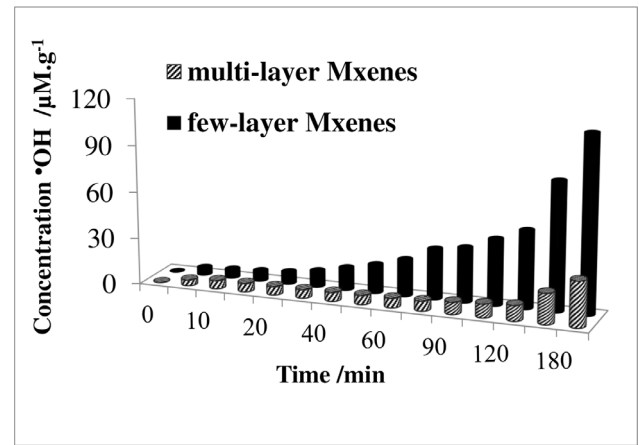


Fig. 6. Quantification of photo-generated hydroxyl radicals by few- and multi-layer Mxene nano-sheets.

pairs, which improves photo-chemical and photocatalytic processes [80,81]. Redox reactions occurring between the dissolved O_2 of the aqueous solution and the $-OH$ surface groups on the Mxene nano-sheets with the photo-generated e^-/h^+ pairs promote the production of ROS such as hydroxyl radicals ($•OH$) [9,82]. Once formed, this reactive specie reacts with the arsenite in the solution thus leading to a lower toxicity-final product, As(V).

In this regard, Fig. 6 shows the quantification of hydroxyl radicals for few- and multi-layer Mxene nano-sheets. It can be clearly observed that the amount of photogenerated hydroxyl radicals for the few-layer Mxene nano-sheets is significantly increased compared to the amount detected for the multi-layer Mxene nano-sheets. This goes hand in hand with the photocatalytic performance observed. The enhanced hydroxyl radical's generation observed for the few-layer Mxene nano-sheets is likely due to its higher amount of available active sites of TiO_2 , which provide more redox reaction sites. Thus, it can be proposed that the photo-oxidation process of As(III) to As(V) is initiated by the presence of ROS in the reaction medium, mostly by radicals $•OH$ [76,83]. The relationship between the photocatalytic activity (assessed by the apparent photo-oxidation rate constant (k_{app})) and the generated amount of $•OH$ radicals is depicted in Fig. 7. In this figure, it can be observed that the photo-oxidation rate is mainly related to the concentration of generated $•OH$ radicals. In this regard, a di-

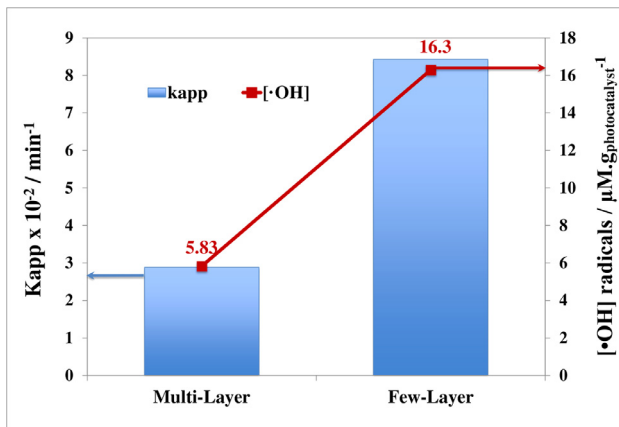


Fig. 7. Relationship between the apparent photo-oxidation rate constant and the amount of photogenerated $•\text{OH}$ radicals for few- and multi-layer Mxene nano-sheets after a reaction time of 45 min.

rect linear relation between the photocatalytic activity and the ROS production can be established, which aligns well with previously published research works [8, 9]. It can be assumed that the higher ROS generation explains the superior photo-oxidation ability of the few-layer Mxene nano-sheets. As a consequence, photo-generated $•\text{OH}$ radicals play a key role in this oxidation process [83].

With respect to the photo-generated As(V), Fig. 4 also shows that, in presence of multi-layer MXene nano-sheets, all As(V) generated by the As(III) oxidation is completely released into the solution. In contrast, when few-layer MXene nano-sheets were used as photocatalyst, only a fraction of As(V) was found in the treated water solution. From these results, it becomes evident that approximately 61% of photo-generated arsenate were adsorbed on few-layer MXene nano-sheet surface. The adsorption capacity of few-layer Mxene nano-sheets related to the negatively charged As(V) specie (HAsO_4^{2-}) could be attributed to the formation of an arsenate bidentate complex between the oxoanion HAsO_4^{2-} and the -OH groups exposed on the surface, rather than electrostatic interactions or physisorption processes, as explained above [83,84].

Based upon our results, it can be clearly seen that the investigated few-layer Mxene nano-sheets can not only efficiently photo-oxidize As(III) to As(V), but also possess a notable adsorption capability for both As species. It must be pointed out that the dual effect of adsorption/photocatalytic oxidation abilities has been only observed for the few-layer Mxene nano-sheets, which makes them a promising material for removing arsenic from water based upon its simultaneous photocatalysis-adsorption capabilities.

4. Conclusions

This study addressed for the first time the photo-oxidative performance of few- and multi-layer $\text{Ti}_3\text{C}_2\text{T}_x$ nano-sheets (Mxenes) regarding the Arsenic removal from synthetic arsenic solutions. Based upon the presented results, the following conclusions can be drawn:

- 4- Advanced materials characterization including HR-TEM, XRD and Raman spectroscopy clearly verified the two-dimensional layered structure with layer-by-layer distances of about 900 pm and the existence of -O, -OH and -F terminations for few- and multi-layer Mxene nano-sheets. A detailed XPS analysis demonstrated that the few- and multi-layer Mxene nano-sheets mainly differ in the relative quantity of hydroxides and metal oxide at the surface.
- 4- Without any further illumination, few- and multi-layer Mxene nano-sheets adsorbed about 44 and 20% of the initial As(III)

concentration, respectively. During UVA irradiation, the complete photo-oxidation of As(III) to As(V) was achieved after 45 and 90 min of irradiation for few- and multi-layer Mxene nano-sheets, respectively. Besides the ability to completely photo-oxidize As(III), few-layer Mxene nano-sheets adsorbed outstanding 50% of the generated As(V).

- 4- The unprecedented dual effect observed for few-layer Mxene nano-sheets unifying an efficient photo-oxidation ability from highly toxic As(III) to less harmful As(V) and an outstanding adsorption capability (about 44% for As(III) and 50% for As(V)) makes them an excellent candidate for the As removal of contaminated water. Few-layer Mxene nano-sheets photogenerated 4 times more hydroxyl radicals compared to multi-layer Mxene nano-sheets, which implies that this reactive oxygen species played a critical role in the photo-oxidation process from As(III) to As(V).

Funding

This work was supported by CONICYT within the project Fondecyt 11180121 as well as the VID of the University of Chile in the framework of "U-Inicia UI013/2018". A. García gratefully acknowledges the financial support provided by the Scientific and Technological Development Support Fund (FONDEF-CONICYT, IT19I0006). A. Rosenkranz and B. Wang gratefully acknowledge the financial support of Chinese Academy of Sciences President's International Fellowship Initiative (2020VEC0006).

Authors' contributions

M. Rosales, A. Garcia and A. Rosenkranz conceived the ideas and designed the experiments. M. Rosales carried out the experiments and discussed the results with A. Garcia, F. Gracia and A. Rosenkranz. G. C. SONG, B. WANG and J. H. YU synthesized the MXene samples, which were characterized by R. Espinoza (HR-TEM), V. Fuenzalida (XPS) and A. Rosenkranz (Raman spectroscopy and XRD). A. Rosenkranz, M. Rosales and A. García wrote the manuscript. All authors have reviewed, edited and thoroughly read the manuscript as well as approved its final version.

Data availability statement

The data that support the findings of this study are available from the corresponding author, A. R., upon request.

Author credit statement

Maibelin Rosales: Conceptualization, Formal analysis, Investigation, Writing - original draft, Writing - review & editing **Andreina Garcia:** Conceptualization, Supervision, Funding acquisition, Writing - original draft, Writing - review & editing **Victor M. Fuenzalida:** Investigation **Rodrigo Espinoza-González:** Investigation **Guichen Song:** Investigation **Bo Wang:** Investigation, Supervision, Writing - review & editing **Jinhong Yu:** Investigation, Supervision, Funding Acquisition, Writing - review & editing **Francisco Gracia:** Supervision, Funding Acquisition, Writing - review & editing **Andreas Rosenkranz:** Conceptualization, Formal analysis, Investigation, Supervision, Funding Acquisition, Writing - original draft, Writing - review & editing

Declaration of Competing Interest

The authors declare that they have no known competing financial interests or personal relationships that could have appeared to influence the work reported in this paper.

Acknowledgments

The authors kindly acknowledge the help of Dr. Roberto Villarreal regarding the measurements of the Raman spectra. Prof. Dr. Nestor Escalona and Dr. Elodie Blanco are acknowledged for their help related to the characterization of the surface area. The authors would like to acknowledge Dr. Sebastian Suarez and the Chair of Functional Materials (Saarland University, Germany) regarding the help with respect to the XRD measurements.

References

- [1] D. Mohan, C.U. Pittman Jr., Arsenic removal from water/wastewater using adsorbents - a critical review, *J. Hazard. Mater.* 142 (2007) 1–53. <https://doi.org/10.1016/j.jhazmat.2007.01.006>.
- [2] R. Singh, S. Singh, P. Parihar, V. Pratap Singh, M. Prasad, Arsenic contamination, consequences and remediation techniques: a review, *Ecotox Environ. Safe* 112 (2015) 247–270. <https://doi.org/10.1016/j.ecoenv.2014.10.009>.
- [3] C. Navas-Cárdenas, H. Murillo, M. Rosales, C. Ron, F. Muñoz, Materials Involved in Electrocoagulation Process for Industrial Effluents, Chapter 12, in: New Technologies for Electrochemical Applications, CRC Press/Taylor & Francis Group, 2020, pp. 193–216. <https://doi.org/10.1201/9780429200205-12>.
- [4] J. Wang, T. Zhang, M. Li, Y. Yang, P. Lu, P. Ning, Q. Wang, Arsenic removal from water/wastewater using layered double hydroxide derived adsorbents, a critical review, *RSC Adv.* 8 (2018) 22694–22709. <https://doi.org/10.1039/C8RA03647K>.
- [5] S. Ye, G. Zeng, H. Wu, J. Liang, C. Zhang, J. Dai, W. Xiong, B. Song, S. Wu, J. Yu, The effects of activated biochar addition on remediation efficiency of co-composting with contaminated wetland soil, *Resour. Conserv. Recy.* 140 (2019) 278–285. <https://doi.org/10.1016/j.resconrec.2018.10.004>.
- [6] A. Ibadon, P. Fitzpatrick, Heterogeneous photocatalysis: recent advances and applications, *Catalysts* 3 (2013) 189–218. <https://doi.org/10.3390/catal3010189>.
- [7] I. Ali, M. Suhail, Z.A. Alothman, A. Alwarthan, Recent advances in syntheses, properties and applications of TiO₂ nanostructures, *RSC Adv.* 8 (2018) 30125–30147. <https://doi.org/10.1039/C8RA06517A>.
- [8] T. Zoltan, M.C. Rosales, Yadarola, Reactive oxygen species quantification and their correlation with the photocatalytic activity of TiO₂ (anatase and rutile) sensitized with asymmetric porphyrins, *J. Environ. Chem. Eng.* 4 (2016) 3967–3980. <https://doi.org/10.1016/j.jece.2016.09.008>.
- [9] M. Rosales, T. Zoltan, C. Yadarola, E. Mosquera, F. Gracia, A. Garcia, The influence of the morphology of 1D TiO₂ nanostructures on photogeneration of reactive oxygen species and enhanced photocatalytic activity, *J. Mol. Liq.* 281 (2019) 59–69. <https://doi.org/10.1016/j.molliq.2019.02.070>.
- [10] S.A. Bakar, C. Ribeiro, Nitrogen-doped titanium dioxide: an overview of material design and dimensionality effect over modern applications, *J. Photoch. Photobio. C* 27 (2016) 1–29. <https://doi.org/10.1016/j.jphotochemrev.2016.05.001>.
- [11] D. Lu, P. Fang, J. Ding, M. Yang, Y. Cao, Y. Zhou, K. Peng, K.K. Kondamareddy, M. Liu, Two-dimensional TiO₂-based nanosheets co-modified by surface-enriched carbon dots and Gd₂O₃ nanoparticles for efficient visible-light-driven photocatalysis, *Appl. Surf. Sci.* 396 (2017) 185–201. <https://doi.org/10.1016/j.apusc.2016.09.022>.
- [12] M.S. Hassan, T. Amna, S.S. Al-Deyab, H.C. Kim, M.S. Khil, Monodispersed 3D MnWO₄-TiO₂ composite nanoflowers photocatalysts for environmental remediation, *Curr. Appl. Phys.* 15 (2015) 753–758. <https://doi.org/10.1016/j.cap.2015.03.022>.
- [13] Y. Dong, X. Fei, Y. Zhou, Synthesis and photocatalytic activity of mesoporous (001) facets TiO₂ single crystals, *Appl. Surf. Sci.* 403 (2017) 662–669. <https://doi.org/10.1016/j.apusc.2017.01.210>.
- [14] T. Jedskontorn, T. Ueno, N. Saito, M. Hunsom, Mechanistic aspect based on the role of reactive oxidizing species (ROS) in macroscopic level on the glycerol photooxidation over defected and defected-free TiO₂, *J. Photoch. Photobio. A* 367 (2018) 270–281. <https://doi.org/10.1016/j.jphotochem.2018.08.030>.
- [15] A. García, Y. Quintero, N. Vicencio, B. Rodríguez, D. Ozturk, E. Mosquera, T.P. Corales, U.G. Volkmann, Influence of TiO₂ nanostructures on anti-adhesion and photoinduced bactericidal properties of thin film composite membranes, *RSC Adv.* 6 (2016) 82941. <https://doi.org/10.1039/CGR417999A>.
- [16] J. Molina-Reyes, A. Romero-Moran, H. Uribe-Vargas, B. Lopez-Ruiz, J.L. Sanchez-Salas, E. Ortega, A. Ponce, A. Morales-Sanchez, F. Lopez-Huerta, C. Zuñiga-Islas, Study on the photocatalytic activity of titanium dioxide nanostructures: nanoparticles, nanotubes and ultra-thin films, *Catal. Today* 341 (2020) 2–12. <https://doi.org/10.1016/j.cattod.2018.05.033>.
- [17] Y. Quintero, E. Mosquera, J. Diosa, A. Garcia, Ultrasonic-assisted sol-gel synthesis of TiO₂ nanostructures: influence of synthesis parameters on morphology, crystallinity, and photocatalytic performance, *J. Sol-Gel. Sci. Tech.* 94 (2020) 477–485. <https://doi.org/10.1007/s10971-020-05263-6>.
- [18] K. Nakata, A. Fujishima, TiO₂ photocatalysis, Design and applications, *J. Photoch. Photobio. C* 13 (2012) 169–189. <https://doi.org/10.1016/j.jphotochemrev.2012.06.001>.
- [19] D. Lu, M. Yang, K.K. Kumar, P. Wu, K. Peng, Facile synthesis of TiO₂-based nanosheets by the regulation of cationic surfactants for effective adsorption-photocatalytic removal of high-chroma crystal violet, *Adv. Pow. Tech.* 29 (2018) 756–764. <https://doi.org/10.1016/j.apt.2017.12.021>.
- [20] M. Deng, X. Wu, A. Zhu, Q. Zhang, Q. Liu, Well-dispersed TiO₂ nanoparticles anchored on Fe₃O₄ magnetic nanosheets for efficient arsenic removal, *J. Environ. Manage.* 237 (2019) 63–74. <https://doi.org/10.1016/j.jenvman.2019.02.037>.
- [21] L. Ren, Y. Li, J. Hou, J. Bao, M. Mao, M. Zeng, X. Zhao, N. Li, The pivotal effect of the interaction between reactant and anatase TiO₂ nanosheets with exposed {001} facets on photocatalysis for the photocatalytic purification of VOCs, *Appl. Catal. B-Environ.* 181 (2016) 625–634. <https://doi.org/10.1016/j.apcatb.2015.08.034>.
- [22] F. Chen, K. Zhu, G. Li, D. Lu, P. Fang, Y. Li, A novel synthesis of ultrathin TiO₂-based nanosheets with excellent photocatalytic performance, *Mater. Lett.* 164 (2016) 516–519. <https://doi.org/10.1016/j.matlet.2015.11.057>.
- [23] J. Yang, Z. Wen, X. Shen, J. Dai, Y. Li, Y. Li, Comparative study on the photocatalytic behavior of graphene-TiO₂ nanostructures: effect of TiO₂ dimensionality on interfacial charge transfer, *Chem. Eng. J.* 334 (2018) 907–921. <https://doi.org/10.1016/j.cej.2017.10.088>.
- [24] M. Naguib, V.N. Mochalin, M.W. Barsoum, Y. Gogotsi, 25th anniversary article: MXenes: a new family of two-dimensional materials, *Adv. Mater.* 26 (2014) 992–1005. <https://doi.org/10.1002/adma.201304138>.
- [25] B. Anasori, M.R. Lukatskaya, Y. Gogotsi, 2D metal carbides and nitrides (MXenes) for energy storage, *Nat. Rev. Mater.* 2 (2017) 16098. <https://doi.org/10.1038/natrevmats.2016.98>.
- [26] J.C. Lei, X. Zhang, Z. Zhou, Recent advances in MXene: preparation, properties, and applications, *Front. Phys.* 10 (2015) 276–286. <https://doi.org/10.1007/s11467-015-0493-x>.
- [27] V.M.H. Ng, H. Huang, K. Zhou, P.S. Lee, W. Que, J.Z. Xu, L.B. Kong, Recent progress in layered transition metal carbides and/or nitrides (MXenes) and their composites: synthesis and applications, *J. Mater. Chem. A* 5 (2017) 3039–3068. <https://doi.org/10.1039/C6TA06772G>.
- [28] D. Xiong, X. Li, Z. Bai, S. Lu, Recent advances in layered Ti₃C₂T_x MXene for electrochemical energy storage, *Small* 14 (2018) 1703419. <https://doi.org/10.1002/smll.201703419>.
- [29] L. Verger, V. Natu, M. Carey, M.W. Barsoum, M. Xenes, An introduction of their synthesis, select properties, and applications, *Trends Chem.* 1 (2019) 656–669. <https://doi.org/10.1016/j.trechm.2019.04.006>.
- [30] R.M. Ronchi, J.T. Arantes, S.F. Santos, Structure Synthesis, properties and applications of MXenes: current status and perspectives, *Ceram. Int.* 45 (2019) 18167–18188. <https://doi.org/10.1016/j.ceramint.2019.06.114>.
- [31] Y. Gogotsi, B. Anasori, The rise of MXenes, *ACS Nano* 13 (2019) 8491–8494. <https://doi.org/10.1021/acsnano.9b06394>.
- [32] A. Sarycheva, Y. Gogotsi, Raman spectroscopy analysis of structure and surface chemistry of Ti₃C₂T_x MXene, *Chem. Mater.* 32 (2020) 3480–3488. <https://doi.org/10.1021/acs.chemmater.0c00359>.
- [33] Y. Xie, Y. Dall'Agnese, M. Naguib, Y. Gogotsi, M.W. Barsoum, H.L. Zhuang, P.R. Kent, Prediction and characterization of MXene nanosheet anodes for non-lithium-ion batteries, *ACS Nano* 8 (2014) 9606–9615. <https://doi.org/10.1021/nn503921j>.
- [34] X. Wang, S. Kajiyama, H. Iinuma, E. Hosono, S. Oro, I. Moriguchi, M. Okubo, A. Yamada, Pseudocapacitance of MXene nanosheets for high-power sodium-ion hybrid capacitors, *Nat. Comm.* 6 (2015) 1–6. <https://doi.org/10.1038/ncomms7544>.
- [35] X. Xie, M.Q. Zahro, B. Anasori, K. Maleski, C.E. Ren, J. Li, B.W. Byles, E. Pomerantseva, G. Wang, Y. Gogotsi, Porous heterostructured MXene/carbon nanotube composite paper with high volumetric capacity for sodium-based energy storage devices, *Nano Energy* 26 (2016) 513–523. <https://doi.org/10.1016/j.nanoen.2016.06.005>.
- [36] J. Yan, C.E. Ren, K. Maleski, C.B. Hatter, B. Anasori, P. Urbankowski, A. Sarycheva, Y. Gogotsi, Flexible MXene/graphene films for ultrafast supercapacitors with outstanding volumetric capacitance, *Adv. Func. Mater.* 27 (2017) 1701264. <https://doi.org/10.1002/adfm.201701264>.
- [37] S. Kajiyama, L. Szabova, K. Sodeyama, H. Iinuma, R. Morita, K. Gotoh, K.Y. Tateyama, M. Okubo, A. Yamada, Sodium-ion intercalation mechanism in MXene nanosheets, *ACS Nano* (2016) 3334–3341. <https://doi.org/10.1021/acsnano.5b06958>.
- [38] Z.W. Seh, K.D. Fredrickson, B. Anasori, J. Kibsgaard, A.L. Strickler, M.R. Lukatskaya, Y. Gogotsi, T.F. Jarillo-Herrero, Two-dimensional molybdenum carbide (MXene) as an efficient electrocatalyst for hydrogen evolution, *ACS Energy Lett.* 1 (2016) 589–594. <https://doi.org/10.1021/acsenergylett.6b00247>.
- [39] J. Ran, G. Gao, F.T. Li, T.Y. Ma, A. Du, S.Z. Qiao, Ti₃C₂ MXene catalyst on metal sulfide photo-absorbers for enhanced visible-light photocatalytic hydrogen production, *Nat. Comm.* 8 (2017) 13907. <https://doi.org/10.1038/ncomms13907>.
- [40] W. Lian, Y. Mai, C. Liu, L. Zhang, S. Li, X. Jie, Two-dimensional Ti₃C₂ coating as an emerging protective solid-lubricant for tribology, *Ceram. Int.* 44 (2018) 20154–20162. <https://doi.org/10.1016/j.ceramint.2018.07.309>.
- [41] A. Rosenkranz, P.G. Grützmacher, R. Espinoza, V.M. Fuenzalida, E. Blanco, N. Escalona, F.J. Gracia, R. Villarreal, L. Guo, R. Kang, F. Mücklich, Z. Zhang, Multi-layer TiCT-nanoparticles (MXenes) as solid lubricants—Role of surface terminations and intercalated water, *Appl. Surf. Sci.* 494 (2019) 13–21. <https://doi.org/10.1016/j.apsusc.2019.07.171>.
- [42] X. Yin, J. Jin, X. Chen, A. Rosenkranz, J. Luo, Ultra-Wear-Resistant MXene-Based Composite Coating via In Situ Formed Nanostructured Tribofilm, *ACS Appl. Mater. Interf.* 11 (2019) 32569–32576. <https://doi.org/10.1021/acsm.9b11449>.
- [43] M. Marian, S. Tremmel, S. Wartzack, G. Song, B. Wang, J. Yu, A. Rosenkranz, MXene nanosheets as an emerging solid lubricant for machine elements—To-

- wards increased energy efficiency and service life, *Appl. Surf. Sci.* 523 (2020) 146503 <https://doi.org/10.1016/j.apsusc.2020.146503>.
- [44] A.K. Fard, G. McKay, R. Chamoun, T. Rhadfi, H. Preud'Homme, M.A. Atieh, Barium removal from synthetic natural and produced water using MXene as two dimensional (2-D) nanosheet adsorbent, *Chem. Eng. J.* 317 (2017) 331–342 <https://doi.org/10.1016/j.cej.2017.02.090>.
- [45] A. Shahzad, K. Rasool, W. Miran, M. Nawaz, J. Jang, K.A. Mahmoud, D.S. Lee, Two-dimensional Ti_3C_2Tx MXene nanosheets for efficient copper removal from water, *ACS Sustain. Chem. Eng.* 5 (2017) 11481–11488 <https://doi.org/10.1021/acssuschemeng.7b02695>.
- [46] R. Kang, Z. Zhang, L. Guo, J. Cui, Y. Chen, X. Hou, B. Wang, C. Lin, N. Jiang, J. Yu, Enhanced thermal conductivity of epoxy composites filled with 2D transition metal carbides (MXenes) with ultralow loading, *Sci. Rep.* 9 (2019) 1–14 <https://doi.org/10.1038/s41598-019-45664-4>.
- [47] L. Guo, Z. Zhang, M. Li, R. Kang, Y. Chen, G. Song, S. Han, C. Lin, N. Jiang, J. Yu, Extremely high thermal conductivity of carbon fiber/epoxy with synergistic effect of MXenes by freeze-drying, *Compos. Commun.* 19 (2020) 134–141 <https://doi.org/10.1016/j.joco.2020.03.009>.
- [48] G. Song, R. Kang, L. Guo, Z. Ali, X. Chen, Z. Zhang, C. Yan, C. Lin, N. Jiang, J. Yu, Highly flexible few-layer Ti_3C_2 MXene/cellulose nanofiber heat-spreader films with enhanced thermal conductivity, *New J. Chem.* 44 (2020) 7186–7193 <https://doi.org/10.1039/DONJ00672F>.
- [49] A. Tariq, S.I. Ali, D. Akinwande, S. Rizwan, Efficient visible-light photocatalysis of 2D-MXene nanohybrids with Gd^{3+} - and Sn^{4+} -codoped bismuth ferrite, *ACS Omega* 3 (2018) 13828–13836 <https://doi.org/10.1021/acsomega.8b01951>.
- [50] H. Zhang, M. Li, J. Cao, Q. Tang, P. Kang, C. Zhu, M. Ma, 2D $a\text{-Fe}_2O_3$ doped Ti_3C_2 MXene composite with enhanced visible light photocatalytic activity for degradation of Rhodamine B, *Ceram. Int.* 44 (2018) 19958–19962 <https://doi.org/10.1016/j.ceramint.2018.07.262>.
- [51] H. Wang, Y. Wu, T. Xiao, X. Yuan, G. Zeng, W. Tu, S. Wu, H.Y. Lee, Y.Z. Tan, J.W. Chew, Formation of quasi-core-shell In_2S_3 /anatase TiO_2 @metallic $Ti_3C_2T_x$ hybrids with favorable charge transfer channels for excellent visible-light-photocatalytic performance, *Appl. Catal. B-Environ.* 233 (2018) 213–225 <https://doi.org/10.1016/j.apcatb.2018.04.012>.
- [52] Y. Liu, R. Luo, Y. Li, J. Qi, C. Wang, J. Li, X. Sun, L. Wang, Sandwich-like Co_3O_4 /MXene composite with enhanced catalytic performance for Bisphenol A degradation, *Chem. Eng. J.* 347 (2018) 731–740 <https://doi.org/10.1016/j.cej.2018.04.155>.
- [53] X. Xie, N. Zhang, R. Tang, M. Anpo, Y.J. Xu, Ti_3C_2Tx MXene as a Janus cocatalyst for concurrent promoted photoactivity and inhibited photocorrosion, *Appl. Cata. B-Environ.* 237 (2018) 43–49 <https://doi.org/10.1016/j.apcatb.2018.05.070>.
- [54] A. Shahzad, K. Rasool, W. Miran, M. Nawaz, J. Jang, K.A. Mahmoud, D.S. Lee, Heterostructural TiO_2 / $TiCT$ (MXene) for photocatalytic degradation of antiepileptic drug carbamazepine, *Chem. Eng. J.* 349 (2018) 748–755 <https://doi.org/10.1016/j.cej.2018.05.148>.
- [55] N. Liu, N. Lu, Y. Su, P. Wang, X. Quan, Fabrication of $g\text{-C}_3N_4/Ti_3C_2$ composite and its visible-light photocatalytic capability for ciprofloxacin degradation, *Sep. Purif. Technol.* 211 (2019) 782–789 <https://doi.org/10.1016/j.seppur.2018.10.027>.
- [56] X. Ding, Y. Li, C. Li, W. Wang, L. Wang, L. Feng, D. Han, 2D visible-light-driven $TiO_2@Ti_3C_2/g\text{-C}_3N_4$ ternary heterostructure for high photocatalytic activity, *J. Mater. Sci.* 54 (2019) 9385–9396 <https://doi.org/10.1007/s10853-018-03289-4>.
- [57] Q. Huang, Y. Liu, T. Cai, X. Xia, Simultaneous removal of heavy metal ions and organic pollutant by $BiOBr/Ti_3C_2$ nanocomposite, *J. Photoch. Photobio. A* 375 (2019) 201–208 <https://doi.org/10.1016/j.jphotochem.2019.02.026>.
- [58] C. Peng, et al., Hybrids of two-dimensional Ti_3C_2 and TiO_2 Exposing {001} facets toward enhanced photocatalytic activity, *ACS Appl. Mater. Interfaces* 8 (9) (2016) 6051–6060.
- [59] C. Peng, X. Yang, Y. Li, H. Yu, H. Wang, F. Peng, Two-dimensional titanium carbide for efficiently reductive removal of highly toxic chromium(VI) from water, *ACS Appl. Mater. Interf.* 7 (2015) 1795–1803 <https://doi.org/10.1021/acsmami.5b11973>.
- [60] R.K. Dhar, Y. Zheng, J. Rubenstein, A. van Geen, A rapid colorimetric method for measuring arsenic concentrations in groundwater, *Anal. Chim. Acta* 526 (2004) 203–209 <https://doi.org/10.1016/j.aca.2004.09.045>.
- [61] A. García, B. Rodríguez, Y. Quintero, Patent Application INAPI No. CL2018001987, Material, method and system for arsenic removal in water, Universidad de Chile 2018. <https://patents.google.com/patent/CL2018001987A1/es?oq=CL2018001987>.
- [62] K. Ishibashi, A. Fujishima, T. Watanabe, K. Hashimoto, Quantum yields of active oxidative species formed on TiO_2 photocatalyst, *J. Photoch. Photobio. A* 134 (2000) 139–142 [https://doi.org/10.1016/S1010-6030\(00\)00264-1](https://doi.org/10.1016/S1010-6030(00)00264-1).
- [63] Y. Liu, X. Zhang, S. Dong, Z. Ye, Y. Wei, Synthesis and tribological property of Ti_3C_2Tx nanosheets, *J. Mater. Sci.* 52 (2017) 2200–2209 <https://doi.org/10.1007/s10853-016-0509-0>.
- [64] M. Cao, F. Wang, L. Wang, W. Wu, W. Lv, J. Zhu, Room temperature oxidation of Ti_3C_2 MXene for supercapacitor electrodes, *J. Electrochem. Soc.* 164 (2017) A3933–A3942 <https://doi.org/10.1149/2.1541714jes>.
- [65] T. Hu, J. Wang, H. Zhang, Z. Li, M. Hu, X. Wang, Vibrational properties of Ti_3C_2 and $Ti_3C_2T_x$ ($T = O, F, OH$) monosheets by first-principles calculations: a comparative study, *Phys. Chem. Chem. Phys.* 17 (2015) 9997–10003 <https://doi.org/10.1039/C4CP05666C>.
- [66] M. Hu, T. Hu, Z. Li, Y. Yang, R. Cheng, J. Yang, C. Cui, X. Wang, Surface functional groups and interlayer water determine the electrochemical capacitance of Ti_3C_2Tx MXene, *ACS Nano* 12 (2018) 3578–3586 <https://doi.org/10.1021/acsnano.8b00676>.
- [67] X. Zhang, Y. Liu, S. Dong, Z. Ye, Y. Guo, One-step hydrothermal synthesis of a $TiO_2\text{-}Ti_3C_2Tx$ nanocomposite with small sized TiO_2 nanoparticles, *Ceram. Int.* 43 (2017) 11065–11070 <https://doi.org/10.1016/j.ceramint.2017.05.151>.
- [68] J.F. Moulder, W.F. Stickle, P.E. Sobol, K.D. Bomben, *Handbook of X-Ray Photoelectron Spectroscopy*, Perkin-Elmer Corporation, Minnesota, 1992.
- [69] J. Halim, K.M. Cook, M. Naguib, P. Eklund, Y. Gogotsi, J. Rosen, M.W. Barsoum, X-ray photoelectron spectroscopy of select multi-layered transition metal carbides (MXenes), *Appl. Surf. Sci.* 362 (2016) 406–417 <https://doi.org/10.1016/j.apsusc.2015.11.089>.
- [70] M.V. Kuznetsov, S.V. Borisov, O.P. Shepatkovskii, Y.G. Veksler, V.L. Kozhevnikov, Investigation of $TiC-C$ coatings by X-ray photoelectron spectroscopy, *J. Surf. Invest.-X-Ray+ 3* (2009) 331–337 <https://doi.org/10.1134/S102745100903001X>.
- [71] T. Tanuma, H. Okamoto, K. Ohnishi, S. Morikawa, T. Suzuki, Partially fluorinated metal oxide catalysts for a Friedel-Crafts-type reaction of dichlorofluoromethane with tetrafluoroethylene, *Catal. Lett.* 136 (2010) 77–82 <https://doi.org/10.1007/s10562-009-0197-3>.
- [72] I.P. Asanov, V.M. Paasonen, L.N. Mazalov, A.S. Nazarov, A. S., X-ray photoelectron study of fluorinated graphite intercalation compounds, *J. Struct. Chem.* 39 (1998) 928–932 <https://doi.org/10.1007/BF02903607>.
- [73] A.A. Galuska, J.C. Uht, N. Marquez, Reactive and nonreactive ion mixing of Ti films on carbon substrates, *J. Vac. Sci. Technol. A* 6 (1988) 110–122 <https://doi.org/10.1116/1.574992>.
- [74] A.V. Naumkin, K.-V. Anna, W.G. Stephen, C.J. Powell, NIST Standard Reference Database 20, Version 4.1 <http://dx.doi.org/10.18434/T4T88K>.
- [75] M.C. Biesinger, L.W. Lau, A.R. Gerson, R.S.C. Smart, Resolving surface chemical states in XPS analysis of first row transition metals, oxides and hydroxides: Sc, Ti, V, Cu and Zn, *Appl. Surf. Sci.* 257 (2010) 887–898 <https://doi.org/10.1016/j.apsusc.2010.07.086>.
- [76] P.K. Dutta, A.K. Ray, V.K. Sharma, F.J. Millero, Adsorption of arsenate and arsenite on titanium dioxide suspensions, *J. Colloid Interface Sci.* 278 (2004) 270–275 <https://doi.org/10.1016/j.jcis.2004.06.015>.
- [77] M. Pena, X. Meng, G.P. Korfiatis, C. Jing, Adsorption mechanism of arsenic on nanocrystalline titanium dioxide, *Environ. Sci. Technol.* 40 (2006) 1257–1262 <https://doi.org/10.1021/es052040e>.
- [78] Y. Li, X. Cai, J. Guo, P. Na, UV-induced photoactive adsorption mechanism of arsenite by anatase TiO_2 with high surface hydroxyl group density, *Colloid. Surf. A* 462 (2014) 202–210 <https://doi.org/10.1016/j.colsurfa.2014.09.011>.
- [79] Y. Huang, W. Zhang, M. Zhang, X. Zhang, Y. Zhao, Hydroxyl-functionalized $TiO_2@SiO_2@Ni/nZVI$ nanocomposites fabrication, characterization and enhanced simultaneous visible light photocatalytic oxidation and adsorption of arsenite, *Chem. Eng. J.* 338 (2018) 369–382 <https://doi.org/10.1016/j.cej.2018.01.019>.
- [80] S. Ye, M. Yan, X. Tan, J. Liang, G. Zeng, H. Wu, B. Song, C. Zhou, Y. Yang, H. Wang, Facile assembled biochar-based nanocomposite with improved graphitization for efficient photocatalytic activity driven by visible light, *Appl. Catal. B Environ.* 250 (2019) 78–88 <https://doi.org/10.1016/j.apcatb.2019.03.004>.
- [81] H. Huang, Y. Song, N. Lia, D. Chena, Q. Xu, H. Li, J. He, J. Lu, One-step in-situ preparation of N-doped $TiO_2@C$ derived from Ti_3C_2 MXene for enhanced visible-light driven photodegradation, *Appl. Catal. B Environ.* 251 (2019) 154–161 <https://doi.org/10.1016/j.apcatb.2019.03.066>.
- [82] K. Nakata, A. Fujishima, TiO₂ photocatalysis, Design and applications, *J. Photoch. Photobio. C* 13 (2012) 169–189 <https://doi.org/10.1016/j.jphotochemrev.2012.06.001>.
- [83] P.K. Dutta, S.O. Pekkanen, V.K. Sharma, A.K. Ray, Photocatalytic oxidation of Arsenic(III): evidence of hydroxyl radicals, *Environ. Sci. Technol.* 39 8 (2005) 1827–1834 <https://doi.org/10.1021/es0489238>.
- [84] S. Bang, M. Patel, L. Lippincott, X. Meng, Removal of arsenic from groundwater by granular titanium dioxide adsorbent, *Chemosphere* 60 (2005) 389–397 <https://doi.org/10.1016/j.chemosphere.2004.12.008>.